2,5-Thiophene Substituted Spirobisiloles - Synthesis, Characterization, Electrochemical Properties and Performance in Bulk Heterojunction Solar Cells

Kassem Amro, Anil K. Thakur, Joëlle Rault-Berthelot, Cyril Poriel, Lionel Hirsch, William Elliott Douglas, Philippe Gerbier, Sébastien Clément

NJC

RSC Publishing

PAPER

View Article Online
View Journal | View Issue

Cite this: *New J. Chem.*, 2013, **37**, 464

2,5-Thiophene substituted spirobisiloles – synthesis, characterization, electrochemical properties and performance in bulk heterojunction solar cells†

Kassem Amro,[a] Anil K. Thakur,[b] Joëlle Rault-Berthelot,[c] Cyril Poriel,[c] Lionel Hirsch,[b] William E. Douglas,[a] Sébastien Clément*[a] and Philippe Gerbier*[a]

Received (in Montpellier, France) 22nd June 2012,
Accepted 6th November 2012

DOI: 10.1039/c2nj40535k

www.rsc.org/njc

New spirobisilole molecules containing thienyl (**DTSBS**) and bis-thienyl (**BBTSBS**) electron donor groups have been synthesized for use as the donor material in bulk-heterojunction solar cells together with PCBM. The spectroscopic, electrochemical and thermal properties of **DTSBS** and **BBTSBS** have been investigated. All these new spirobisiloles exhibit excellent thermal stability. Cyclic voltammetry measurements revealed reversible and irreversible oxidation and irreversible reduction processes. The highest occupied and lowest unoccupied molecular orbital (HOMO/LUMO) energy levels were determined from electrochemical measurements and DFT calculations. The HOMO/LUMO energy levels were estimated to lie in the range of −5.2 to −2.3 eV for **DTSBS** and −4.9 to −2.6 eV for **BBTSBS**. For both compounds, electropolymerization processes occur at potentials higher than 1.5 V leading to low band gap electrogenerated polymers. Spin-coating-deposited bulk-heterojunction solar cells fabricated with the novel spirobisiloles as donor and PCBM as acceptor displayed open-circuit voltages up to 0.4 V, short-circuit currents around 0.5 mA cm^{-2}, and power conversion efficiencies approaching 0.1%.

Introduction

Fossil fuel exhaustion and environmental problems caused by conventional power generation have triggered an intensification of research on renewable energies such as photovoltaic sources, fuel cells, wind generation, *etc.* In particular, photovoltaic conversion of solar energy is considered to be one of the most significant ways of addressing the growing global energy crisis. To this end, organic solar cells (OSCs) represent a promising candidate for the conversion of solar energy owing to their advantages of easy fabrication, low cost, light weight and flexibility. Different device architectures of OSCs have been developed since the pioneering work of Tang in 1986.[1] The most efficient cell design, leading to the highest power conversion efficiencies (PCEs), is the bulk-heterojunction (BHJ) solar cell.[2]

The active layer of BHJ solar cells consists of an interpenetrating network of two types of organic materials, an electron donor and an electron acceptor, and is formed through the control of the phase separation between the donor and acceptor parts in the bulk. Accordingly, the large donor–acceptor area can favour charge separation and, hence, increases the conversion efficiency of the cell. For both small molecule and polymer based BHJ solar cells, controlling the microscopic morphology plays an important role in creating domains of donor and acceptor material of optimal dimensions consistent with exciton diffusion while ensuring the transport of holes and electrons without interruption in their respective domains.[3,4] At a basic level, control of the blend morphology can be achieved by tailoring the various fabrication methods such as the choice of the solvent, the solvent evaporation rate, the thermal annealing treatment *etc.* On a deeper level, control consists in modulating the

[a] *Institut Charles Gerhardt Montpellier ICGM, UMR 5253, CNRS-UM2-ENSCM-UM1, Equipe CMOS, Université Montpellier 2, Bâtiment 17, CC 1701. Place E. Bataillon, 34095 Montpellier Cedex 5, France. E-mail: sebastien.clement02@univ-montp2.fr, philippe.gerbier@univ-montp2.fr; Fax: +33 4 6714 3852; Tel: +33 4 6714 4501*

[b] *Université de Bordeaux, Laboratoire IMS, UMR CNRS 5218, Ecole Nationale Supérieure de Chimie, Biologie et Physique, 16 Avenue Pey Berland, 33607 Pessac Cedex, France*

[c] *Université de Rennes 1, CNRS UMR 6226, Institut des Sciences Chimiques de Rennes - MaCSE group, Bat. 10C, Campus de Beaulieu, 35042 Rennes Cedex, France*

† Electronic supplementary information (ESI) available: ^{1}H and $^{29}Si\{^{1}H\}$ NMR spectra of **DTSBS**, **BBTSBS**, TGA traces for **DTSBS** and **BBTSBS**, experimental DPV recorded in CH_2Cl_2–$[NBu_4][PF_6]$ in the presence of **DTSBS** and **BBTSBS**, cyclic voltammetry in CH_2Cl_2–$[NBu_4][PF_6]$ in the presence of **DTSBS** and **BBTSBS**, cyclic voltammetry in CH_2Cl_2–$[NBu_4][PF_6]$ of **poly(BBTSBS)** and **poly(DTSBS)** deposited on a platinum electrode, UV visible spectroscopy of neutral, slightly p-doped and highly p-doped **poly(BBTSBS)** electrogenerated by anodic oxidation of **BBTSBS** on an ITO glass electrode. See DOI: 10.1039/c2nj40535k

molecular structure of the conjugated molecular materials,[5] this being essential as it affects not only the molecular ordering in thin solid films but also the conjugation length, light absorption, carrier mobilities, exciton dynamics and processability. Therefore, to date, much attention has been devoted to the synthesis of new donor and acceptor materials for OSCs applications.

In the fields of both small-molecule and polymer solar cells, an enormous increase in power conversion efficiencies has been achieved in recent years, from under 1% initially to currently over 8.3%.[1,6] Recently, a certified PCE of 9.8% has been achieved by a tandem cell manufactured with an oligomer-material low-temperature deposition process. Small conjugated molecules are attractive for OSCs since compared to their polymeric counterparts, they are easier to synthesize and purify, offer higher charge-carrier mobilities than do polymers and, most importantly, avoid the problems posed by batch variations in the case of polymers.[5a–c]

One strategy for improving OSCs efficiency based on small-molecule donors consists in increasing the dimensionality of the donor molecules through self-assembly to match the intrinsically three-dimensional (3D) character of intermolecular interactions in the fullerene acceptor phase and to ensure 3D hole transport.[5a,7] Therefore, the synthesis of conjugated systems possessing a pseudo-3D geometry has been the subject of intense research over the last decade.[8] Roncali *et al.* first reported a tetrahedral molecular donor based on a silicon-centred system exhibiting a PCE of 0.3%.[9] Similar donor systems with increased dimensionality based on X-shaped or dendritic oligothiophene have achieved PCE $\approx$ 1.5%.[10]

Although these 3D architectures provide motifs for the most isotropic charge-transport properties, the most efficient aggregation can be achieved with two-dimensional (2D) π–π stacking in mutually orthogonal interactions. Such stacking interactions can be obtained from cross-conjugated molecules where the two mutually conjugated backbones connected through a central aromatic core or an sp^3-hybridized atom into a spiro configuration undergo self-assembly in the third dimension.[7,11] The two perpendicularly-orientated chromophores joined through a C, Si or Ge spiro-centre in cross-conjugated cruciform molecules are usually considered to be independent despite spiro interactions being known.[12] Recently, Samuel *et al.* have exploited this approach for OSC application by using a fused spirobi[(1,3,2)dithiagermole]quinquithiophene system. This Ge cruciform molecule demonstrated an improved mobility and a maximum PCE of 2.26%.[7]

In this respect, we report the synthesis, thermal, photophysical and electrochemical properties of two spirobisiloles with an increasing number of thienyl units for use in OSCs. To the best of our knowledge, although such compounds have been used as electron transport materials in the construction of electroluminescent devices, they have never been utilized in OSCs.[13] Only one example of a photovoltaically active silole has been reported in the literature.[14] These new spirobisiloles were then used as donors with [6,6]-phenyl-C61-butyric acid methyl ester (PCBM) as an acceptor in BHJ solar cells exhibiting power conversion efficiencies over 0.1%. Our results suggest that spirobisiloles are promising materials for developing efficient solution-processed BHJ solar cells based on small molecules.

Results and discussion

Synthesis of DTSBS and BBTSBS

The two spirobisilole derivatives were synthesized in moderate yield *via* a one-pot synthesis involving first the intramolecular reductive cyclization of 1,1-bis(phenylethynyl)-2,3,4,5-tetraphenylsilole, followed by a palladium-catalyzed cross-coupling reaction with the appropriate bromoaryl compound, as shown in Scheme 1.[13a]

DTSBS and **BBTSBS** were isolated in 30–35% yield as yellow-orange and dark red powders, respectively. The characterization of **DTSBS** and **BBTSBS** was achieved by means of elemental analysis and standard spectroscopic techniques (see NMR spectra, Fig. S1–S4, ESI†). The most relevant structural data for these compounds arise from the characteristic downfield shift of the ^{29}Si NMR signal ($\approx$1 ppm), compared with bis(phenylethynyl)-diphenylsilane (−47.9 ppm).[13b,15]

Thermal stability is of crucial importance for evaluating the suitability of a molecule for photovoltaic applications. Hence, the thermal properties were investigated by thermogravimetric analysis (TGA) and differential scanning calorimetry (DSC) under an inert atmosphere at a heating rate of 10 °C min^{-1} (Fig. S5 and S6, ESI†). Both spirobisilole compounds display good thermal stability since the first weight losses upon heating occur at temperatures exceeding 230 °C. In addition, the DSC traces indicate no glass transition for either **DTSBS** or **BBTSBS** between 30 °C and the decomposition temperature.

Electronic and luminescence properties in solution

The optical properties of **DTSBS** and **BBTSBS** were studied by absorption and fluorescence spectroscopy (Table 1). The characteristic absorption spectra of **DTSBS** and **BBTSBS** in solution are shown in Fig. 1A (for thin film characteristics, see Fig. S7, ESI†).

DTSBS and **BBTSBS** exhibit two and three absorption bands, respectively. The first-absorption band in the 250–300 nm

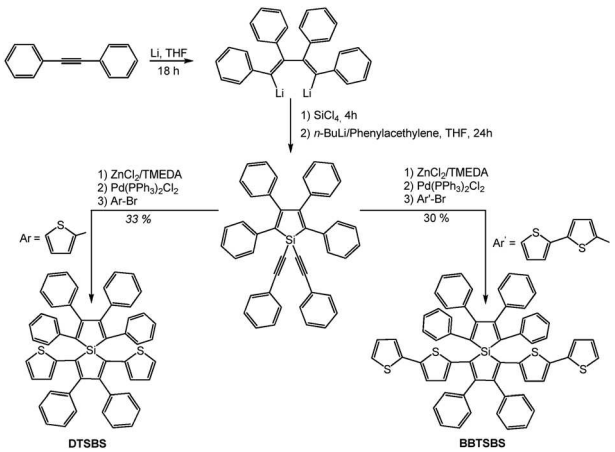

Scheme 1

Table 1 Absorption and emission properties of **DTSBS** and **BBTSBS**

Compound	λ_{abs} (nm)	ε^a (L mol^{-1} cm^{-1})	λ_{em} (THF)^b (nm)	λ_{em} (solid) (nm)	$\phi_F{}^c$ (THF)
DTSBS	400	16 600	520	570	0.20
BBTSBS	384	19 100	625	665	0.32
	494	18 600			

^{a} Molar absorptivity. ^{b} Excitation at λ_{abs}. ^{c} Luminescence quantum yield relative to 9,10-diphenylanthracene for **DTSBS** and cresyl violet for **BBTSBS**.

region is ascribed to the π–π* transition of the aromatic groups. Based on previous theoretical and experimental investigation on a 2,5-functional silole, the second and the third broad low-energy absorption bands, for **BBTSBS**, can be attributed to the electronic transition between the highest occupied molecular orbital (HOMO) including a π orbital involving contributions from both the silole ring and the aromatic substituents at the 2,5 positions and the lowest unoccupied molecular orbital (LUMO), the latter being a pure π* orbital from the silole ring.[13a,16] The optical band-gap energies of **DTSBS** and **BBTSBS**, estimated from the edge of the absorption spectrum (455 nm for **DTSBS** and 580 nm for **BBTSBS** in Fig. 1A) using $\Delta E_{opt} = hc/\lambda$(nm), are *ca.* 2.73 and 2.13 eV, respectively.

When irradiated by UV light, both compounds emit both in solution (Fig. 1B) and in the solid state (Fig. S8, ESI†) (Table 1). In order to exclude possible effects of self-absorption, the measurements in solution were performed at low concentration (10^{-5} M). The emission spectra in CH_2Cl_2 (Fig. 1B) show broad unstructured bands at λ_{max} at 520 nm and 625 nm for **DTSBS** and **BBTSBS**, respectively. Both the absorption and the luminescence maxima of **BBTSBS** are shifted to longer wavelengths with respect to **DTSBS** owing to the increased number of the thienyl units.[17] The emission quantum efficiency for these two compounds is low in solution (<1%), as is common for silole derivatives.[13a,16]

To examine the potential aggregation-induced emission (AIE) properties of these new spirobisilole derivatives, PL spectra of **DTSBS** and **BBTSBS** in THF–water mixtures were measured. Since **DTSBS** and **BBTSBS** are insoluble in water, they must have aggregated in THF–water mixtures with increasing water content. Fig. 2A and B shows the photoluminescence decrease with increasing water content. These results clearly indicate that both silole derivatives are AIE-inactive. Tang *et al.* have proposed that the restriction of the intramolecular rotation (RIR) process accounts for the AIE effect.[18] On the basis of the very rigid molecular structure of spirobisilole compounds **DTSBS** and **BBTSBS**, we assume that the intramolecular rotation of the phenyl and thiophene is extremely restricted in solution and is not very different from that of aggregates. Such a behaviour for **DTSBS** and **BBTSBS** may probably account for their failure to display the AIE effect.

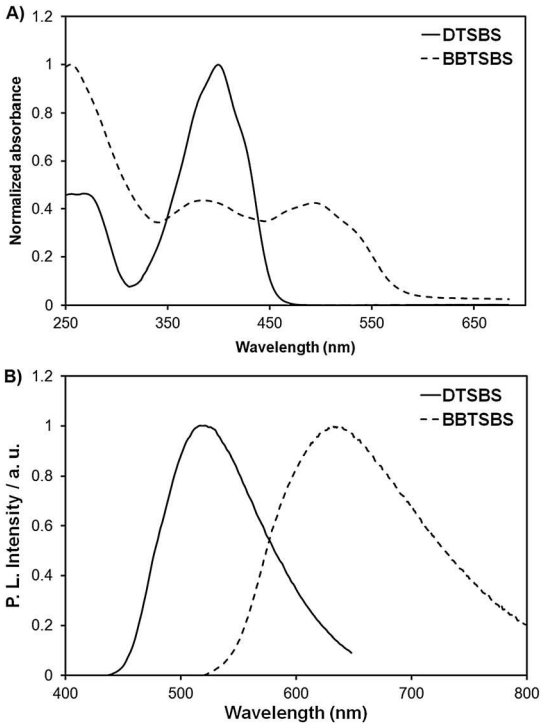

Fig. 1 Absorption and emission spectra of **DTSBS** and **BBTSBS** (10^{-5} M) in CH_2Cl_2.

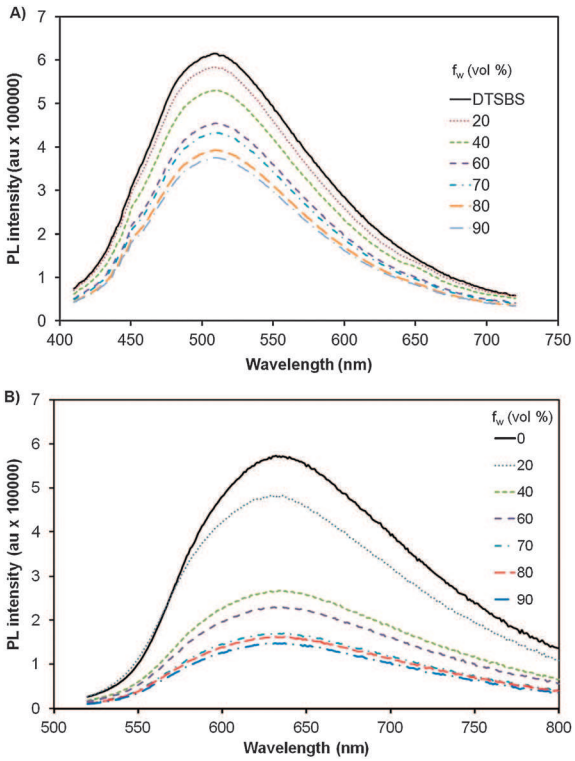

Fig. 2 PL spectra of **DTSBS** (A) and **BBTSBS** (B) in THF–water mixtures with different water fractions (f_w). Excitation wavelength at λ_{abs}.

Theoretical calculations

Very few structural studies on spirobisiloles have been reported to date reflecting their very low propensity for crystallization. Both **DTSBS** and **BBTSBS** follow this rule. For this reason, density functional theory (DFT) calculations with the UB3LYP

functional were carried out on these molecules to obtain information about their molecular conformations. Geometry optimizations without symmetry constrains were performed with the 6-31G basis set to the standard convergence criteria as implemented in Gaussian 03.[19] Such calculations were followed by single point runs using a 6-31+G* basis with tight convergence and the ultrafine integration grid in order to obtain accurate energies. Prior to analysis, the methodology was tested using the crystallographically characterized octaphenyl-1,1′-spirobisilole (**OPSBS**)[20] and 2,5-dithienylsiloles (**DTS** and **BBTS**)[21] to verify if the optimized geometry is in good agreement with the X-ray data (Scheme 2).

The optimized structures of both **DTSBS** and **BBTSBS** exhibit the previously observed anti-coplanar arrangement of the 2,5-dithiophene or bis-bithienyl moieties to the central silole ring.[21] The twist angles between the two thienyl mean planes and the silole mean plane are 5.9° for **DTSBS** and 3.9° for **BBTSBS**, respectively. The overall structures are very close to that of the parent octaphenyl-1,1′-spirobisilole (**OPSBS**) with a nearly perfect perpendicular arrangement between the adjacent silole rings.[20] The energy diagrams of the frontier orbitals shown in Fig. 3 summarize the results obtained for single point DFT calculations performed on optimized geometries as described above for a series of relevant silole derivatives (see also Fig. S11, ESI†). For the siloles **TPS**, **DTS**, **BBTS** and for the spirobisilole **OPSBS**, only HOMO and LUMO orbital energy levels are shown. For the spirobisiloles **DTSBS** and **BBTSBS**, the HOMO − 1 and LUMO + 1 energy levels are also shown in addition to those of the HOMO and LUMO. As reported elsewhere, the electronic perturbation afforded by the substituents located at the 2,5-positions has a pronounced effect on both the HOMO and the LUMO energy levels.[22] For instance, replacement of the phenyls (**TPS**) by electron-rich thienyl (**DTS**) or bis-thienyl (**BBTS**) groups leads to both a substantial decrease of the LUMO level and an increase in the HOMO level. These changes also reflect the fact that the replacement of a benzene ring by the less sterically hindering thiophene ring gives rise to a more planar conformation of the conjugated backbone. The same trend is also observed when **OPSBS**, **DTSBS** and **BBTSBS** are compared. Also of interest is the comparison of the LUMO + 1, LUMO, HOMO and HOMO − 1 energy levels of **DTSBS** and **BBTSBS** with the HOMO–LUMO energy levels of **OPSBS**, **DTS** and **BBTS**: the HOMO–LUMO energy levels of

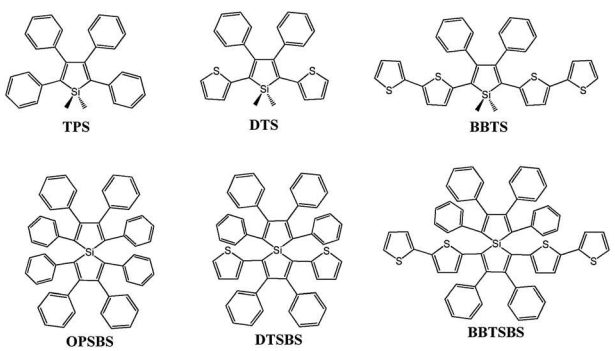

Scheme 2

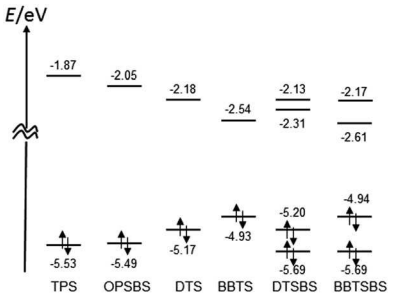

Fig. 3 Energy diagram of frontier orbitals of siloles and spirobisiloles estimated from B3LYP/6-31G* calculations.

DTSBS are close to those of **DTS** whereas the (HOMO + 1)–(LUMO − 1) energy levels are close to those of **OPSBS** (being in the range of those calculated for **TPS**). The same effect is observed for **BBTSBS**.

The orbital plots (Fig. 4) for **BBTSBS** are typical for the HOMO and LUMO orbitals of siloles, *i.e.* the LUMO of the silole ring displays typical $\sigma(Si–C_{exocyclic})^*–\pi(butadiene)^*$ hyperconjugation responsible for its remarkable electronic properties.[22,23]

As can be seen in Fig. 4, the HOMO spreads over the π-system bearing the bis-thienyl moieties, whereas the HOMO − 1 spreads over the orthogonal π-system (see also Fig. S17, ESI†), thus indicating that there is no mixing between these frontier orbitals. This is in contrast to the parent **OPSBS** (see inset Fig. 4) and other symmetric spirobisiloles in which the orbital clouds spread in a symmetrical fashion over the two rings (Fig. S11 and S13, ESI†).[23] Looking now at the LUMO (Fig. S14, ESI†), the orbital mainly spreads over the silole bearing the bis-thienyl moieties, but in this case, since the $\sigma(Si–C_{orthogonal\ silole})^*$ orbital is involved in the LUMO (see above), a small part of the cloud is also present on the orthogonal silole ring. The reverse of this situation is also

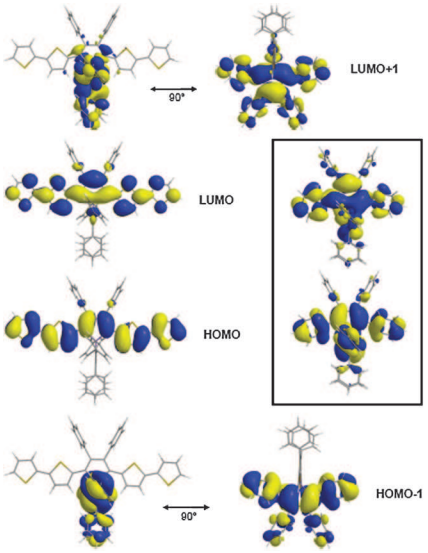

Fig. 4 Kohn–Sham frontier orbitals of **BBTSBS** and **OPSBS** (inset).

encountered for the LUMO + 1. Therefore, the two rings interact with each other through mutual σ(Si–$C_{orthogonal\ silole}$)*–π(butadiene) hyperconjugation in the LUMO and LUMO + 1 orbitals.

Finally, the question of the existence of spiroconjugation in both **DTSBS** and **BBTSBS** is discussed. Spiroconjugation in spiro-connected π-systems may occur when the frontier orbitals of the fragments with the correct symmetry interact with each other to form two spiroconjugated orbitals (Fig. S11 and S12, ESI†).[23–25] If the spiroconjugation is the result of a HOMO–HOMO interaction, a slight increase of the HOMO energy of the spiro molecule is thus observed in comparison to the energy the HOMO of the constitutive fragments. On the other hand, if the spiroconjugation is the result of a LUMO–LUMO interaction, a slight decrease in the LUMO energy of the spiro molecule is observed. Since no mixing is expected for the LUMO orbitals without the correct symmetry, only HOMO–HOMO spiroconjugation is encountered for the symmetric spirobisiloles **OPSBS** and **TTSBS** (Fig. S11, ESI†) where the effective mixing of the HOMO yields spiroconjugated orbitals spanning the entire molecule. On the contrary, such spiroconjugation is not observed in either **DTSBS** or **BBTSBS** since there is no mixing of the π-orbitals located on the two orthogonal rings either in the HOMO or HOMO − 1 levels. This may originate from the very large energy difference between the HOMO levels of the constitutive fragments.

In summary, theoretical calculations showed definitely that because of a great energy difference between the frontier orbitals of each half of the spirobisiloles, spiroconjugation occurs neither in **DTSBS** nor in **BBTSBS**. From this point of view, they may be described as being independent of each other rather than electronically coupled. However, since the two rings interact with each other through mutual σ(Si–$C_{orthogonal\ silole}$)*–π(butadiene) hyperconjugation one cannot exclude communication between the two halves.

Electrochemical properties

The electrochemical properties of **DTSBS** and **BBTSBS** were investigated by cyclic voltammetry (CV) and differential pulse voltammetry (DPV). The first oxidation of **DTSBS** is irreversible, (see inset of Fig. 5A) and occurs with a maximum at 1.0 V. This first oxidation is followed at higher potentials by at least five ill-defined irreversible processes. The electrochemical behaviour of **BBTSBS** (Fig. 5B) is different from that of **DTSBS** as its oxidation occurs first through three reversible oxidations with maxima at 0.75, 0.9 and 1.15 V (see inset of Fig. 5B) followed by two irreversible oxidation waves. The onset oxidation potential (E^{ox}_{onset}) was observed at 0.88 V and 0.61 V for **DTSBS** and **BBTSBS**, respectively. The 150 mV shift to a lower anodic value of E^{ox}_{onset} for **BBTSBS** is in accordance with the more extended conjugation in **BBTSBS** compared to **DTSBS**. The intensities of the different oxidation waves have been compared using DPV for both compounds (Fig. S15, ESI†). For **DTSBS**, the three first oxidation waves are in the ratio $1e^-/2e^-/3e^-$ whereas the oxidation of **BBTSBS** occurs through three successive one-electron processes followed by a third two

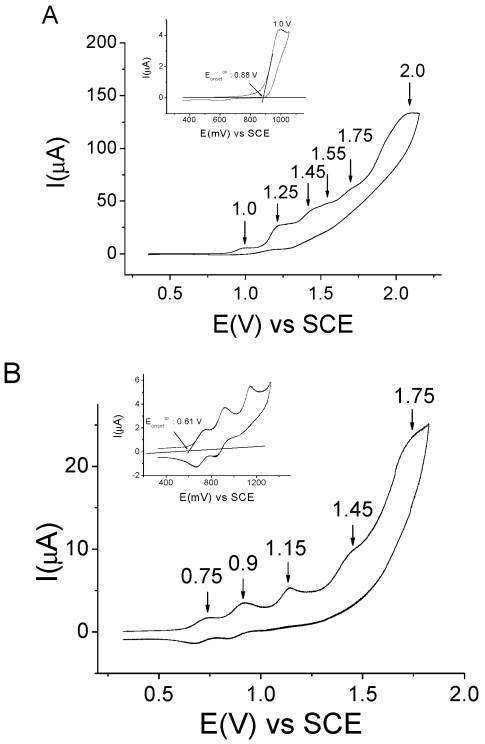

Fig. 5 Cyclic voltammetry in CH_2Cl_2–$[NBu_4][PF_6]$ (0.2 M) of **DTSBS** (9.8×10^{-3} M) in (A) and of **BBTSBS** (3.2×10^{-3} M) in (B). One cycle between 0.4 and 2.15 V in (A) and 0.3 and 1.85 V in (B). Insets show zooms of the first oxidation process in (A) and of the three first oxidation processes in (B). Working electrode: 1 mm diameter Pt disk, sweep-rate: 100 mV s^{-1}.

electron oxidation. It should be noted that for both compounds oxidation at potentials higher than 1.5 V leads to the electrode being covered by insoluble deposits resulting from an electropolymerization process. Reduction of both compounds gives two irreversible reduction waves with maxima around −2.0 and −2.3 V for **DTSBS** and −1.65 and −2.1 V for **BBTSBS** (Fig. S16, ESI†). The onset reduction potentials (E^{red}_{onset}) occur at −1.8 V for **DTSBS** and at −1.55 V for **BBTSBS**. The 250 mV shift towards less cathodic potentials for **BBTSBS** E^{red}_{onset} is also in accordance with the more extended conjugation in **BBTSBS** compared to **DTSBS**.

From the redox data, the lowest unoccupied molecular orbital (LUMO) energy level and the highest occupied molecular orbital (HOMO) energy level can be estimated. The value of E^{ox}_{onset} gives a HOMO level energy of −5.28 eV for **DTSBS** (DFT calculations: −5.21 eV) and −5.01 eV (DFT calculations: −4.94 eV) for **BBTSBS**. The LUMO energy levels of **DTSBS** and **BBTSBS** have also been calculated from E^{red}_{onset} to be −2.6 eV and −2.85 eV respectively (DFT calculations: −2.31 eV and −2.61 eV, respectively). The electrochemical bandgaps (ΔE_{el}) for both compounds were calculated from the HOMO and LUMO levels to be 2.68 eV for **DTSBS** and 2.16 eV for **BBTSBS**. These ΔE_{el} values are in accordance with the optical bandgaps (ΔE_{opt} = 2.73 eV for **DTSBS** and 2.13 eV for **BBTSBS**) determined previously. The difference between the two ΔE_{el} values (0.52 eV) is also in good agreement with the 0.56 eV difference observed between the theoretical bandgaps (ΔE_{theo}) (ΔE_{theo} = 2.89 eV for

DTSBS and 2.33 eV for **BBTSBS**, see Fig. 3). The physicochemical properties of a series of 2,5-diarylsiloles, in particular those of 1,1-dimethyl-3,4-diphenyl-2,5-di(2-thienyl)silole (**DTS**) and 1,1-dimethyl-3,4-diphenyl-2,5-bis[5-(2-thienyl)-2-thienyl]silole (**BBTS**), these being half parts of **DTSBS** and **BBTSBS**, have been reported by Tamao *et al.*[22] The oxidation and reduction potentials of **DTS** are less anodic and less cathodic than those of **BBTS** owing to the extended conjugation with increasing numbers of thienyl units in the main aromatic skeleton. The shift of the oxidation (−90 mV) and the reduction (+170 mV) potentials from **DTS** to **BBTS** were however smaller than those observed in the present study (−250 mV for oxidation and +350 mV for reduction). This electronic effect may be perhaps amplified by the presence of the second aromatic unit in the case of **BBTSBS** and **DTSBS**. As shown from the theoretical calculations (see above), this electronic effect may be the result of the mutual $\sigma(Si–C_{orthogonal\ silole})^*–\pi$(butadiene) hyperconjugation between the silole rings present in **BBTSBS** and **DTSBS**.

Polymerization process

As presented in the previous section, oxidation of **BBTSBS** and **DTSBS** occurs through successive oxidation processes and, for both compounds, oxidation at potentials higher than 1.5 V gives rise to an electropolymerization process. Fig. 6A and B presents the evolution of the CVs recorded for **BBTSBS** and **DTSBS** oxidation performed with recurrent sweeps between −0.5 and 1.56 or 1.50 V, respectively.

In each case, large increases in the oxidation and reduction currents are observed indicating the deposition of insoluble electroactive **poly(BBTSBS)** and **poly(DTSBS)** on the platinum surfaces. Both films are insoluble in common solvents (CH_2Cl_2, THF, DMF, acetone, acetonitrile, MeOH). The modified electrodes rinsed with CH_2Cl_2 and studied by CV in monomer-free solution demonstrate the electrochemical behaviour of the electrogenerated polymers showing in the anodic range (inset, Fig. 6A and B) a p-doping process with very good reversibility. The onset oxidation potentials of the polymers (Fig. 6C) are recorded at 36 mV and 166 mV for **poly(BBTSBS)** and **poly(DTSBS)** cathodically shifted by 575 and 714 mV, respectively, when compared to the onset oxidation potentials of their parent monomers (E^{ox}_{onset}: 0.61 and 0.88 V, respectively, insets, Fig. 5A and B). The large shift suggests a longer conjugation pathway in the polymer than in the monomer. Both polymers can also be obtained by oxidation at a fixed potential, the best value being determined by chronoamperometry. In the cathodic direction (Fig. S17, ESI†), the polymers do not present any reversible n-doping processes, their reductions starting at −1.61 and −1.85 V respectively. These polymer reduction potentials are only slightly shifted towards cathodic potentials compared to their respective monomers (E^{red}_{onset}: −1.55 and −1.8 V, Fig. S16, ESI†).

Despite the absence of a reversible n-doping process, the electroactivity of both polymers remains stable even after cathodic explorations. The presence of the thienyl or dithienyl units in **DTSBS** and **BBTSBS** may offer an explanation for the polymerization process. In fact, one of the most versatile routes

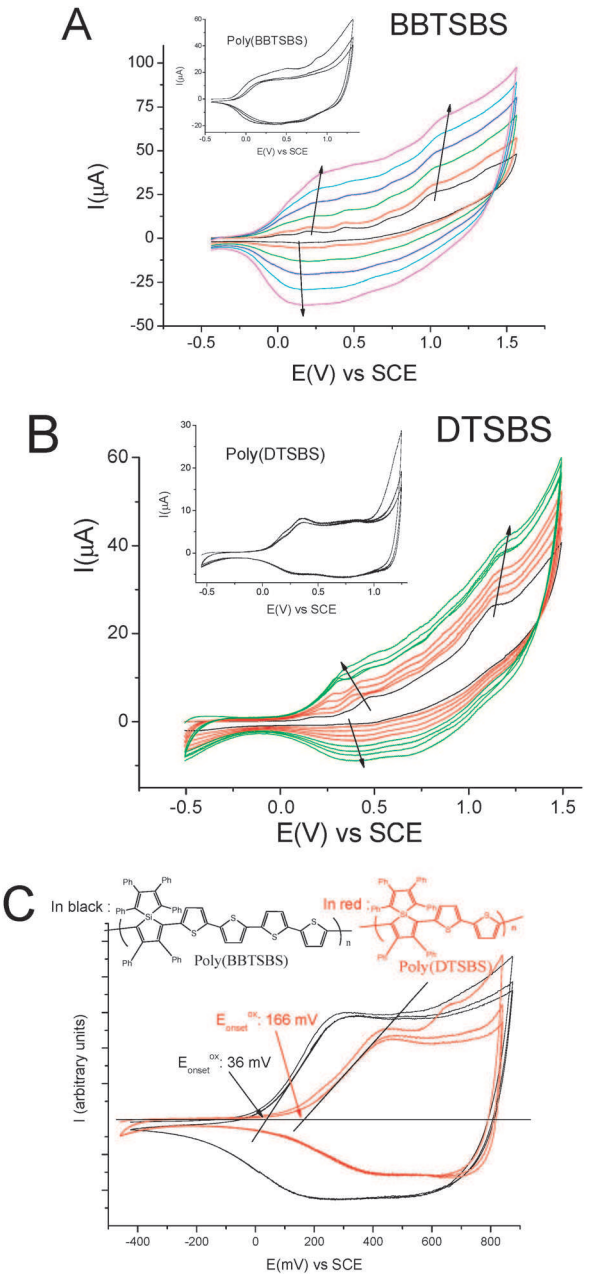

Fig. 6 Cyclic voltammograms in dry CH_2Cl_2 containing Bu_4NPF_6 (0.2 M) and Al_2O_3; (A) in the presence of **BBTSBS** (5×10^{-3} M), 6 sweeps between −0.5 and 1.56 V; (B) in the presence of **DTSBS** (5×10^{-3} M), 9 sweeps between −0.5 and 1.5 V working electrode: platinum disk (*d*) 1 mm. Inset in (A) and (B), the working electrode is a platinum disk (*d*) 1 mm coated by poly(**BBTSBS**) or poly(**DTSBS**) prepared in (A) and (B), respectively, and the solution is free of monomer. (C) Comparison of the p-doping processes of **poly(BBTSBS)** and **poly(DTSBS)** in solutions free of monomer. Sweep-rate: 100 mV s^{-1}.

toward π-conjugated polymers involves the electropolymerization of thienyl units *via* an oxidation process involving coupling of radical cations.

The oxidation of the phenyl units occur at higher potential values than the oxidation of the thienyl or dithienyl units, the polymerization processes may be assigned essentially to thienyl–thienyl couplings leading to the polymers depicted as

in Fig. 6C.[26,27] The HOMO and LUMO levels of the two polymers were calculated from their respective oxidation and reduction threshold potentials. For **poly(DTSBS)**, the HOMO (−4.44 eV) and LUMO (−2.55 eV) values give an electrochemical bandgap of 1.89 eV and for **poly(BBTSBS)**, the HOMO of −4.57 eV and the LUMO of −2.79 eV give a bandgap of 1.77 eV. Due to their relatively low bandgaps, these electrogenerated polymers may be of interest in bulk heterojunction solar cells with the appropriate acceptor.[28] UV-visible spectra of the polymers electrodeposited on a transparent ITO glass electrode show that they absorb light throughout the wavelength range between 300 and 1000 nm (Fig. S18, ESI†). Moreover, both polymers also present interesting electrochromic properties, depicted for **poly(BBTSBS)** in Fig. S18 (ESI†). For example, **poly(BBTSBS)** is pink in its neutral and slightly p-doped state whereas it appears blue in its higher p-doped state exhibiting evolution of its absorbance spectrum with progressive oxidation (Fig. S18, ESI†).

Photovoltaic properties

The **BBTSBS** and **DTSBS** were used as electron-donor materials in bulk-heterojunction solar cells with [6,6]-phenyl-C61 butyric acid methyl ester (PCBM) as an electron acceptor. The cells were prepared by spin-coating a solution (3% w/v) of **DTSBS** or **BBTSBS** and PCBM onto an ITO/PEDOT:PSS substrate. The thickness of the blended film was found to be ≈100 nm. A 100 nm thick Al electrode was then evaporated inside the glove-box for both geometries. The blend ratio of donor to acceptor was 1 : 1 by weight. Fig. 7 and 8 show the *J*–*V* characteristics of bulk hetero-junction (BHJ) **DTSBS** and **BBTSBS** based solar cells.

A thermal treatment has been carried out in order to control the phase separation of the blend. Fig. 7 shows the photovoltaic characteristics of bulk hetero-junctions solar cells based on **DTSBS** and PCBM annealed at different temperatures for 20 minutes. It can be seen that the open circuit voltage (V_{OC}) increases and the short-circuit current (J_{SC}) decreases as the annealing temperature increases (Table 2).

The optimum annealing temperature has been found to be 140 °C for 20 minutes. The increased V_{OC} is due to the reduced recombination rate. The low fill factor values are related to a very high series resistance, which prevents charge collection at the electrodes. Leakage currents are also high as evidenced by the low on/off ratio of dark current which also contributes to lowering V_{OC}. The decrease in fill factor and J_{SC} are observed because of crystallization of PCBM which reduces the effective active area of the solar cell.

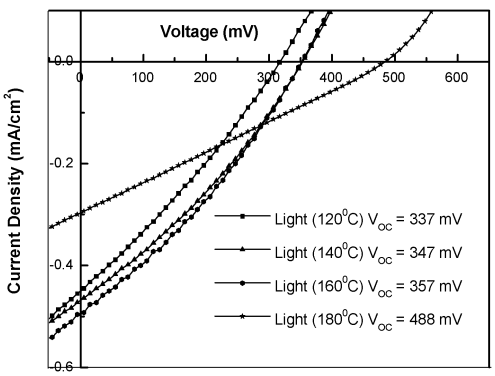

Fig. 7 The photovoltaic characteristics of **DTSBS**:PCBM solar cells annealed at different temperatures for 20 minutes.

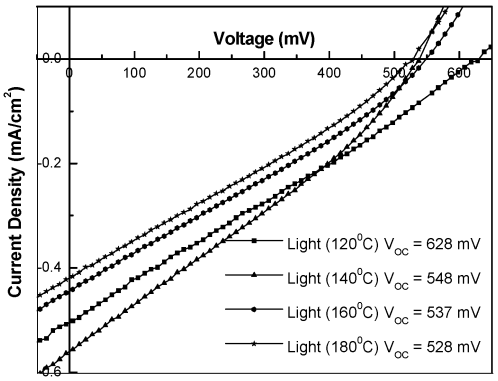

Fig. 8 The photovoltaic characteristics of **BBTSBS**:PCBM solar cells annealed at different temperatures for 20 minutes.

Table 2 The photovoltaic parameters of **DTSBS**:PCBM solar cells

Annealing temperature (°C)	V_{OC} (mV)	J_{SC} (mA cm^{-2})	Fill factor (%)	On/off ratio of dark current (±1 Volt)	Efficiency (η)
120	337	0.45	26.9	1.12	0.04
140	347	0.47	31.5	7.46	0.05
160	357	0.49	31.2	8.45	0.05
180	488	0.29	26.1	4.76	0.03

Fig. 8 shows the photovoltaic characteristics of bulk hetero-junctions solar cells based on **BBTSBS** and PCBM annealed at different annealed temperatures for 20 minutes. It can be seen that the open circuit voltage (V_{OC}) and the short-circuit current (J_{SC}) decrease as the annealing temperature increases (Table 3). The optimum annealing temperature was found to be 120 °C for 20 minutes. The high series resistance prevents efficient charge collection due to recombination and implies a low fill factor. These materials are promising for photovoltaic applications since they exhibit high V_{OC} in the case of **BBTSBS**:PCBM and high repeatability for **DTSBS**:PCBM. However, charge collection is not efficient and progresses should be made in controlling the phase separation of the blend.

Table 3 The photovoltaic parameters of **BBTSBS**:PCBM solar cells

Annealing temperature (°C)	V_{OC} (mV)	J_{SC} (mA cm^{-2})	Fill factor (%)	On/off ratio of dark current (±1 Volt)	Efficiency (η)
120	628	0.56	29.1	17.7	0.10
140	548	0.51	31.4	14.4	0.08
160	537	0.44	29.3	10.4	0.06
180	528	0.42	28.0	8.76	0.06

Table 4 Mobility of **DTSBS**:PCBM blended solar cells after annealing at different temperatures

Annealing temperature (°C)	Slope	Mobility ($cm^2\ V^{-1}\ s^{-1}$)
120	4.32	1.45×10^{-6}
140	26.43	8.90×10^{-6}
160	31.28	1.05×10^{-5}
180	33.70	1.13×10^{-5}

Table 5 Mobility of **BBTSBS**:PCBM blended solar cells after annealing at different temperatures

Annealing temperature (°C)	Slope	Mobility ($cm^2\ V^{-1}\ s^{-1}$)
120	1.64	5.53×10^{-7}
140	1.69	5.69×10^{-7}
160	1.73	5.83×10^{-7}
180	2.03	6.84×10^{-7}

Both low current and high series resistances indicate that numerous dead ends are present rather than a continuous interpenetrated network. The mobility of **DTSBS** and **BBTSBS** has been extracted from dark currents according to the space charged limited current (SCLC) model (Tables 4 and 5.[29]

The low mobility observed in the two materials is consistent with the relatively low efficiency of the solar cells and has to be enhanced in order to balance the electron mobility in PCBM as has recently been demonstrated in the well-known P3HT–PCBM blend.[30]

Conclusion

In summary, we have prepared spirobisiloles containing thienyl (**DTSBS**) and bis-thienyl (**BBTSBS**) substituents for small-organic solar cells. The structures and purity were fully characterized by NMR, mass and elemental analysis. All these new organic materials exhibit excellent thermal stability. On the basis of theoretical calculations, spiroconjugation occurs neither in **DTSBS** nor in **BBTSBS** owing to a large energy difference between the frontier orbitals of each half of the spirobisiloles. However, since the two rings interact with each other through mutual $\sigma(Si–C_{orthogonal\ silole})^*–\pi$(butadiene) hyperconjugation, communication between the two halves certainly takes place. Appropriate positions of their HOMO and LUMO levels make possible their use in bulk heterojunction photovoltaic cells with $PC_{60}BM$ as the electron acceptor component. Preliminary results leading to modest power conversion efficiencies of ~0.1% have been determined for the devices obtained by spin-coating. Further improvements of the devices based on these materials could include optimization of the film as well as the choice of other solvents during the deposition process.

The electrochemical properties of these new materials also revealed for both compounds the occurrence of electropolymerization processes leading to low band gap (1.89 eV and 1.77 eV for **poly(DTSBS)** and **poly(BBTSBS)** respectively) electrogenerated polymers. These polymers exhibit wide absorption spectra covering the wavelength range between 300 and 1000 nm. Owing to these interesting properties, **poly(DTSBS)** and **poly(BBTSBS)** may be of interest in bulk-heterojunction polymer solar cells with the appropriate acceptor. The study of their physicochemical properties is in progress and will be reported shortly.

Experimental

Materials

All reactions were carried out under argon using standard high vacuum and Schlenk techniques. 5-Bromo-2,2′-bithiophene and bis(phenylethynyl)-2,3,4,5-tetraphenylsilole were prepared according to literature methods.[31,32] 2-Bromothiophene (Acros, 98%) was used without further purification. Solvents were dried and distilled just before use.

General procedure for the synthesis of DTSBS and BBTSBS

A mixture of lithium (6.6 mmol) and naphthalene (6.6 mmol) in 5 mL of THF was stirred at room temperature under argon for 4 h giving a deep dark-green solution of lithium naphthalenide. A solution of bis(phenylethynyl)-2,3,4,5-tetraphenylsilole (1.7 mmol) in 10 mL of THF was added dropwise to the solution of lithium naphthalenide for 2 min at room temperature. After being stirred for 5 min, the mixture was cooled to 0 °C and $ZnCl_2$·tmeda (6.6 mmol) was added at 0 °C, followed by dilution with 10 mL of THF. The resulting black suspension was stirred for one additional hour at room temperature. Then, a solution of the bromoaryl compound (Ar–Br, Ar = thiophene or bithiophene) (3.3 mmol) in 5 mL of THF and $Pd(PPh_3)_2Cl_2$ (0.05 mmol) was added. The mixture was refluxed for 18 h. After the mixture was cooled to room temperature, an aqueous solution (100 mL) of 1 M HCl was added and the mixture was extracted with CH_2Cl_2. The combined extracts were washed with brine, dried over $MgSO_4$ and the organic solvent was removed under reduced pressure. The residue was purified by column chromatography on silica gel using dichloromethane/pentane (1 : 9) as an eluent affording **DTSBS** and **BBTSBS** as orange and red solids, respectively.

2,3,3′,4,4′,5-Hexaphenyl-2′,5′-bis(2-thienyl)spirobisilole (**DTSBS**). Yield 33%. ^{1}H NMR ($CDCl_3$, δ ppm): 7.26–6.99 (m, 32H, $H_{aromatic}$); 6.90–6.85 (m, 4H, $H_{aromatic}$). $^{13}C\{^1H\}$ NMR ($CDCl_3$, δ ppm): 158.0; 140.4; 139.0; 138.7; 129.7; 129.2; 127.9; 127.8; 127.7; 127.5; 127.3; 126.6; 125.9; 125.7. $^{29}Si\{^1H\}$ NMR ($CDCl_3$, δ ppm): 0.99. UV-Vis (CH_2Cl_2) (λ_{max} nm, log ε): 400 (4.22). HR-MS (ESI-TOF$^+$) $C_{52}H_{37}S_2Si^+$ $[M + H]^+$: calcd m/z = 753.2061; found 753.2106. Elem. anal. (%) $C_{52}H_{37}S_2Si$: calcd C 82.94, H 4.82, S 8.52; found C 82.68, H 4.53, S 8.27.

2,3,3′,4,4′,5-Hexaphenyl-2′,5′-bis(2″,2‴-bithiophen-5″-yl) spirobisilole (**BBTSBS**). Yield 30%. ^{1}H NMR ($CDCl_3$, δ ppm): 7.26–6.89 (m, 40H, $H_{aromatic}$). $^{13}C\{^1H\}$ RMN ($CDCl_3$, δ ppm): 156,4; 141.2; 139.5; 139.0; 137.7; 137.1; 136.3; 129.9; 129.1; 128.8; 127.9; 127.7; 127.0; 126.1; 125.0; 124.8; 124.6; 124.5, 124.0; 123.7; 123.2. $^{29}Si\{^1H\}$ NMR ($CDCl_3$, δ ppm): 1.02. UV-Vis (CH_2Cl_2) (λ_{max} nm, log ε): 384 (4.28), 494 (4.27). HR-MS (ESI-TOF$^+$) $C_{60}H_{41}S_4Si^+$ $[M + H]^+$: calcd m/z = 917.1816; found 917.1860.

Elem. anal. (%) $C_{60}H_{40}S_4Si$: calcd C 78.56, H 4.40, S 13.98; found C 78.39, H 4.30, S 13.72.

Characterization methods

The ^1H, $^{13}C\{^1H\}$ and $^{29}Si\{^1H\}$ nuclear magnetic resonance (NMR) spectra were obtained on a Bruker Advance 200 DPX spectrometer. All the chemical shifts and coupling constants are reported in ppm and Hz, respectively. Abbreviations for ^1H NMR spectra used are as follows: s, singlet; d, doublet; m, multiplet. UV-visible spectra in solution were recorded on a Perkin Elmer Lambda 35 spectrophotometer in quartz cells and CH_2Cl_2 was used as the solvent. Absorption spectra of **DTSBS** and **BBTSBS** in the solid state were measured on a SAFAS UV MC2 spectrophotometer following their evaporation onto sapphire substrates. High resolution mass spectra were recorded on a Q-Tof Waters 2001 MS instrument. Thermogravimetric analyses were carried out on a TA Instruments Q500 with a heating rate of 10 °C min^{-1} under a flow of nitrogen, using Pt crucibles and 10 mg of sample for each analysis. Elemental analyses were determined with a Thermofinigane Flash EA 1112 instrument. The photoluminescence spectra (PL) were recorded with a SPEX Fluorolog spectrometer. All electrochemical experiments were performed under an argon atmosphere, using a Pt disk electrode (diameter 1 mm), the counter electrode was a vitreous carbon rod and the reference electrode was a silver wire in a 0.1 M $AgNO_3$ solution in CH_3CN. Ferrocene was added to the electrolyte solution at the end of a series of experiments. The ferrocene/ferrocenium (Fc/Fc^+) couple served as the internal standard. The three electrode cell was connected to a PAR Model 273 potentiostat/galvanostat (PAR, EG&G, USA) monitored with the ECHEM Software. Activated Al_2O_3 was added to the electrolytic solution to remove excess moisture. All potentials are referred to the SCE electrode that was calibrated at −0.405 V *vs.* the Fc/Fc^+ system. Preparative separations were performed by silica gel flash column chromatography (Baeckeroot-Labo 60 M).

Photovoltaic device fabrication

Bulk-heterojunction solar cells based on spirobisilole (**DTSBS**, **BBTSBS**) compounds and phenyl-C_{61}-butyric acid methyl esters (PCBM) (Aldrich, 99.5%) were fabricated from their blended solution (1:1, 20 mg mL^{-1}) in chlorobenzene by spin-coating on a poly-[ethylenedioxythiophene]:poly(styrenesulfonic acid) (PEDOT:PSS) (≈50 nm) coated ITO glass substrate. The ITO substrate contains four devices of each compound with an area of *ca.* 8.5 mm^2 and has an overall size of 1.5 cm × 1 cm. To investigate the effects of annealing on the photovoltaic performance, unannealed and annealed devices before and after deposition of aluminum electrodes were prepared. Current density–voltage (*J*–*V*) characteristics were recorded using a Keithley 2400 Source meter under an AM1.5 G solar simulator calibrated at 100 mW cm^{-2} using a radiometer (IL 1400BL).

Acknowledgements

The authors thank the CNRS and the Université Montpellier II for financial support. The authors are also grateful to the Agence Nationale de la Recherche for financial support of the research project ANR PSICO.

Notes and references

1 C. W. Tang, *Appl. Phys. Lett.*, 1986, **48**, 183.
2 (*a*) G. Yu, J. Jao, J. C. Hummelen, F. Wudl and A. J. Heeger, *Science*, 1995, **270**, 1789; (*b*) J. J. M. Halls, K. Pichler, R. H. Friend, S. C. Moratti and A. B. Holmes, *Appl. Phys. Lett.*, 1996, **68**, 3120.
3 (*a*) H. Hoppe and N. S. Sariciftci, *J. Mater. Chem.*, 2006, **16**, 45; (*b*) D. Chen, A. Nakahara, D. Wei, D. Nordlund and T. P. Russell, *Nano Lett.*, 2011, **11**, 561; (*c*) P. M. Beaujuge and J. M. J. Fréchet, *J. Am. Chem. Soc.*, 2011, **133**, 20009.
4 (*a*) J. G. Xue, B. P. Rand, S. Uchida and S. R. Forrest, *Adv. Mater.*, 2005, **17**, 66; (*b*) J. Peet, J. Y. Kin, N. E. Coates, W. L. Ma, D. Moses, A. J. Heeger and G. C. Bazan, *Nat. Mater.*, 2007, **6**, 497; (*c*) M. Campoy-Quiles, T. Ferenzi, T. Agostinelli, P. G. Etchegoin, Y. Kim, T. D. Anthopoulos, P. N. Stravrinou, D. D. C. Bradley and J. Nelson, *Nat. Mater.*, 2008, **7**, 158.
5 (*a*) J. Roncali, *Acc. Chem. Res.*, 2009, **42**, 1719; (*b*) B. Walker, C. Kim and T.-Q. Nguyen, *Chem. Mater.*, 2011, **23**, 470; (*c*) A. Mishra and P. Bäuerle, *Angew. Chem., Int. Ed.*, 2012, **51**, 2020; (*d*) Y. Sun, G. C. Welch, W. L. Leong, C. J. Takacs, G. C. Bazan and A. J. Heeger, *Nat. Mater.*, 2012, **11**, 44; X. Zhan and D. Zhu, *Polym. Chem.*, 2010, **1**, 409; (*e*) H. Zhou, L. Yang and W. You, *Macromolecules*, 2012, **45**, 607.
6 (*a*) Y.-J. Cheng, S.-H. Yang and C.-S. Hsu, *Chem. Rev.*, 2009, **109**, 5868; (*b*) S. H. Park, A. Roy, S. Beaupre, S. Cho, N. Coates, J. S. Moon, D. Moses, M. Leclerc, K. Lee and A. J. Heeger, *Nat. Photonics*, 2009, **3**, 297; (*c*) H. Y. Chen, J. Hou, S. Zhang, Y. Liang, G. Yang, Y. Yang, L. Yu, Y. Wu and G. Li, *Nat. Photonics*, 2009, **3**, 649; (*d*) P.-L. T. Boudreault, A. Najari and M. Leclerc, *Chem. Mater.*, 2011, **23**, 456; (*e*) N. Jenny, *Mater. Today*, 2011, **14**, 462; (*f*) M. A. Green, K. Emery, Y. Hishikawa and W. Warta, *Prog. Photovoltaics*, 2011, **19**, 84.
7 I. A. Wright, A. L. Kanibolotsky, J. Cameron, T. Tutle, P. J. Skabara, S. J. Coles, C. T. Howells, A. J. Thomson, S. Gambino and I. D. W. Samuel, *Angew. Chem., Int. Ed.*, 2012, **51**, 4562.
8 A. L. Kanibolotsky, I. F. Perepichka and P. J. Skabara, *Chem. Soc. Rev.*, 2010, **39**, 2695.
9 (*a*) S. Roquet, R. de Bettignies, P. Leriche, A. Cravino and J. Roncali, *J. Mater. Chem.*, 2006, **16**, 3040; (*b*) J. Roncali, P. Frère, P. Blanchard, R. de Bettignies, M. Turbiez, S. Roquet, P. Leriche and Y. Nicolas, *Thin Solid Films*, 2006, **511**, 567.
10 (*a*) E. A. Kleymyuk, P. A. Troshin, E. A. Khakina, Y. N. Luponosov, Y. L. Moskvin, S. M. Peregudova, S. D. Badenko, T. Meyer-Friedrichsen and S. A. Ponomarenko, *Energy Environ. Sci.*, 2010, **3**, 1941; (*b*) H. Shang, H. Fan, Y. Liu, W. Hu, Y. Li and X. Zhan, *J. Mater. Chem.*, 2011, **21**, 9667; (*c*) C.-Q. Ma, M. Fonrodona, M. C. Schikora, M. M. Wienk, R. A. J. Janssen and P. Bäuerle, *Adv. Funct. Mater.*, 2008, **18**, 3323.
11 (*a*) A. J. Zucchero, P. L. McGrier and U. H. F. Bunz, *Acc. Chem. Res.*, 2010, **43**, 397; (*b*) A. Zen, A. Bilge, F. Galbrecht, R. Alle, K. Meerholz, J. Grenzer, D. Neher, U. Scherf and T. Farell, *J. Am. Chem. Soc.*, 2006, **128**, 3914; (*c*) C. Poriel, J.-J. Liang, J. Rault-Berthelot, F. Barriere, N. Cocherel, A. M. Z. Slawin, D. Horhant, M. Virboul, G. Alcaraz, N. Audebrand, L. Vignau, N. Huby, G. Wantz and L. Hirsch, *Chem.–Eur. J.*, 2007, **13**, 10055; (*d*) D. Thirion, C. Poriel, J. Rault-Berthelot, F. Barriere and O. Jeannin, *Chem.–Eur. J.*, 2010, **16**, 13646.
12 T. P. I. Saragi, T. Spehr, A. Siebert, T. Fuhrmann-Lieker and J. Salbeck, *Chem. Rev.*, 2007, **107**, 1011.
13 (*a*) J. Lee, Y.-Y. Yuan, Y. Kang, W.-L. Jia, Z.-H. Lu and S. Wang, *Adv. Funct. Mater.*, 2006, **16**, 681; (*b*) H. Lee, J. Kim and Y. Kang, *Inorg. Chem. Commun.*, 2007, **10**, 731; (*c*) L. C. Palilis, H. Murata, M. Uchida and Z. H. Kafafi, *Org. Electron.*, 2003, **4**, 113.
14 B. Mi, Y. Dong, Z. Li, J. W. Y. Lam, M. Haübler, H. H. Y. Sung, H. S. Kwok, Y. Dong, I. D. Williams, Y. Liu, Y. Luo, Z. Shuai, D. Zhu and B. Z. Tang, *Chem. Commun.*, 2005, 3583.

15 R. Köster, G. Seidel, I. Klopp, C. Krüger, G. Kher, J. Süβ and B. Wrackmeyer, *Chem. Ber.*, 1993, **126**, 1385.
16 (*a*) J. H. Lee, Q. D. Liu, D. R. Bai, Y. J. Kang, Y. Tao and S. Wang, *Chem. Mater.*, 2004, **16**, 1869; (*b*) J. H. Lee, Q. D. Liu, D. R. Bai, Y. J. Kang, Y. Tao and S. Wang, *Organometallics*, 2004, **23**, 6205.
17 X. Zhan, S. Barlow and S. R. Marder, *Chem. Commun.*, 2009, 1948.
18 Y. Hong, J. W. Y. Lama and B. Z. Tang, *Chem. Commun.*, 2009, 4339.
19 M. J. Frisch, G. W. Trucks and H. B. Schlegel, *et al.*, *GAUSSIAN 03*, Wallingford, CT, 2004.
20 D. Yan, J. Mohsseni-Ala, N. Auner, M. Bolte and J. W. Bats, *Chem.–Eur. J.*, 2007, **13**, 7204.
21 S. Yamaguchi, Y. Itami and K. Tamao, *Organometallics*, 1998, **17**, 4910.
22 S. Yamaguchi, T. Endo, M. Uchida, T. Izumizawa, K. Furukawa and K. Tamao, *Chem.–Eur. J.*, 2000, **6**, 1683.
23 T. Agou, Md. D. Hossain and T. Kawashima, *Chem.–Eur. J.*, 2010, **16**, 368.
24 R. Gleiter and W. Schäfer, *Acc. Chem. Res.*, 1990, **23**, 369.
25 P. Maslak, *Adv. Mater.*, 1994, **6**, 405.
26 (*a*) P. M. DiCarmine, X. Wang, B. L. Pagenkopf and O. A. Semenikhin, *Electrochem. Commun.*, 2008, **10**, 229; (*b*) J. C. Byers, P. M. DiCarmine, M. M. Abd Rabo Moustafa, X. Wang, B. L. Pagenkopf and O. A. Semenikhin, *J. Phys. Chem. B*, 2009, **113**, 15715.
27 C. Poriel, Y. Ferrand, P. Le Maux, J. Raul-Berthelot and G. Simmoneaux, *Chem. Commun.*, 2003, 1104.
28 (*a*) P. Sonar, J. P. F. Lim and K. L. Chan, *Energy Environ. Sci.*, 2011, **4**, 1558; (*b*) J. E. Antony, *Chem. Mater.*, 2011, **23**, 583; (*c*) M. Planells and N. Robertson, *Eur. J. Org. Chem.*, 2012, 4947.
29 J. Huang, H. Jia, L. Li, Z. Lu, W. Zhang, W. He, B. Jiang, A. Tang, Z. Tan, C. Zhan, Y. Li and J. Yao, *Phys. Chem. Chem. Phys.*, 2012, **14**, 14238.
30 M. Abbas and N. Tekin, *Appl. Phys. Lett.*, 2012, **101**, 073302.
31 R. Wu, J. S. Schumm, D. L. Pearson and J. M. Tour, *J. Org. Chem.*, 1996, **61**, 6906.
32 J. Chen, C. C. W. Law, J. W. Y. Lam, Y. Dong, S. M. F. Lo, I. D. Williams, D. Zhu and B. Z. Tang, *Chem. Mater.*, 2003, **15**, 1535.